nature structural & molecular biology

Structural insights into the mechanism of abscisic acid signaling by PYL proteins

Ping Yin[1,2,4], He Fan[1,2,4], Qi Hao[1,3,4], Xiaoqiu Yuan[1,3,4], Di Wu[1,2], Yuxuan Pang[1,2], Chuangye Yan[1,2], Wenqi Li[1,3], Jiawei Wang[1,2] & Nieng Yan[1,3]

Abscisic acid (ABA) is an important phytohormone that regulates plant stress responses. Proteins from the PYR-PYL-RCAR family were recently identified as ABA receptors. Upon binding to ABA, a PYL protein associates with type 2C protein phosphatases (PP2Cs) such as ABI1 and ABI2, inhibiting their activity; the molecular mechanisms by which PYLs mediate ABA signaling remain unknown, however. Here we report three crystal structures: apo-PYL2, (+)-ABA-bound PYL2 and (+)-ABA-bound PYL1 in complex with phosphatase ABI1. Apo-PYL2 contains a pocket surrounded by four highly conserved surface loops. In response to ABA binding, loop CL2 closes onto the pocket, creating a surface that recognizes ABI1. In the ternary complex, the CL2 loop is located near the active site of ABI1, blocking the entry of substrate proteins. Together, our data reveal the mechanisms by which ABA regulates PYL-mediated inhibition of PP2Cs.

Abscisic acid (ABA) is a vital hormone that regulates plant growth, leaf abscission, seed and bud dormancy, and stress responses[1–3]. A central question in the investigation of ABA signaling is how this small molecule is sensed. A few protein targets have been reported to be the putative ABA receptors[4–6], yet their biochemical roles remain to be characterized[7,8].

A family of proteins with at least 14 known members in *Arabidopsis thaliana* (**Supplementary Fig. 1**) was recently found to interact with ABA and mediate ABA-dependent association and inhibition of PP2Cs[9,10]. These proteins belong to the plant pathogenesis–related proteins of class 10 (PR-10)[11] and share sequence homology with the star-related lipid-transfer (START) domain[12]. They have been named regulatory component of ABA receptors (RCARs)[9] or pyrabactin resistance 1 (PYR1) and PYR1-like proteins (PYLs)[10]. For simplicity, we will refer to these proteins hereafter as PYLs. Plant PP2Cs, such as ABI1 and ABI2, are known core components in the ABA signaling pathway, repressing ABA signaling at an early step[13–15]. The recent observations that PYLs inactivate PP2Cs in response to ABA signaling suggest that PYLs may be receptors or co-receptors for ABA.

On the basis of known structures of other START family proteins[12], PYLs were predicted to contain a ligand-binding pocket[9,10] that could be a binding site for ABA. The binding affinity between ABA and PYL9 (RCAR1) was found to increase by approximately ten-fold in the presence of phosphatase ABI2 (ref. 9). There are at least two potential models that could account for these observations. An intuitive explanation posits a binding site of ABA shared by PYL9 and ABI2; in this case, ABA could function as a 'molecular glue' to bring together PYL9 and ABI2, but it remains to be seen whether ABA is directly involved in the binding and inhibition of PP2Cs[10]. An alternative explanation is allostery, whereby ABA binding induces conformational changes in PYL9 that create a binding surface for ABI2.

To understand the molecular mechanisms of ABA recognition and ABA-dependent inhibition of PP2Cs by PYLs, we sought to determine the structures of PYLs in isolation, PYLs in complex with ABA, and PYLs bound to ABA and PP2Cs. Toward this goal, we subcloned 14 PYLs and 5 PP2Cs from an *A. thaliana* cDNA library, overexpressed and purified the proteins to homogeneity, and attempted crystallization trials for various complex combinations. In this manuscript, we report the crystal structures of PYL2 in both the apo and (+)-ABA–bound forms as well as that of (+)-ABA–bound PYL1 in complex with the catalytic core domain of ABI1. Guided by the structures, we generated a number of loss-of-function PYL2 mutants. Structural and biochemical analyses indicate that (i) PYLs are ABA receptors rather than co-receptors, (ii) ABA binding induces a conformational change in PYLs that allows subsequent binding of PP2Cs, and (iii) ABA-bound PYLs inhibit PP2Cs by blocking entry of substrate proteins.

RESULTS

Structure of apo-PYL2

The full-length PYL2 was crystallized in the $C222_1$ space group. The structure was determined by iodine-based single-wavelength anomalous dispersion (I-SAD) and refined to a resolution of 1.65 Å (**Fig. 1a** and **Table 1**). There are three molecules in each asymmetric unit, two of which form a homodimer while the third one forms an identical homodimer with a symmetry-related molecule (**Supplementary Fig. 2**). The three molecules within one asymmetric unit are similar to each other, with a pairwise r.m.s. deviation of ~0.3 Å over 174 Cα atoms (**Supplementary Fig. 2c**).

The dimer interface is mediated primarily by van der Waals interactions, together with a few polar contacts and water-mediated hydrogen bonds (**Fig. 1b**). Each protomer contributes at least 13 amino acids toward dimer formation, resulting in the burial of surface area of 1,766 Å^2.

[1]State Key Laboratory of Bio-membrane and Membrane Biotechnology, [2]Center for Structural Biology, School of Life Sciences and [3]School of Medicine, Tsinghua University, Beijing, China. [4]These authors contributed equally to this work. Correspondence should be addressed to N.Y. (nyan@tsinghua.edu.cn).

Received 7 October; accepted 30 October; published online 5 November 2009; doi:10.1038/nsmb.1730

We investigated the existence of a PYL2 dimer in solution by size-exclusion chromatography using a calibrated Superdex-200 HR10/30 column (**Supplementary Fig. 2e**). The wild-type (WT) PYL2 protein, with or without (+)-ABA, eluted at a volume that corresponds to a molecular mass of ~40 kDa, whereas the molecular weight of a PYL2 monomer is ~22 kDa. PYL2 mutants containing either a single mutation (F66A or I88A) or triple mutations (N157A/M164A/F165A) in the dimer interface showed similar elution volume (data not shown). However, a PYL2 variant containing all five mutations had an elution volume corresponding to a molecular mass of ~20 kDa. These observations support the structural finding that PYL2 may exist as a homodimer in solution.

As predicted[9,10], each PYL2 molecule contains a typical helix-grip fold[12], comprising a central seven-stranded β-sheet flanked by two α-helices (α1 and α2) along its concave side (**Fig. 1c**). There is an additional α-helical segment at the N terminus, which we refer to as helix α0 to distinguish it from the helix-grip fold. Sequence analysis of all 14 PYLs revealed four highly conserved surface loops connecting α1 and β2, β3 and β4, β5 and β6, and β7 and α2, which we named CL1, CL2, CL3 and CL4, respectively (**Fig. 1c** and **Supplementary Fig. 1**). These four loops are located on one end of the curved β-sheet and, together with elements of helix α1, strands β3–β7 and helix α2, encircle a highly conserved pocket (**Fig. 1d**).

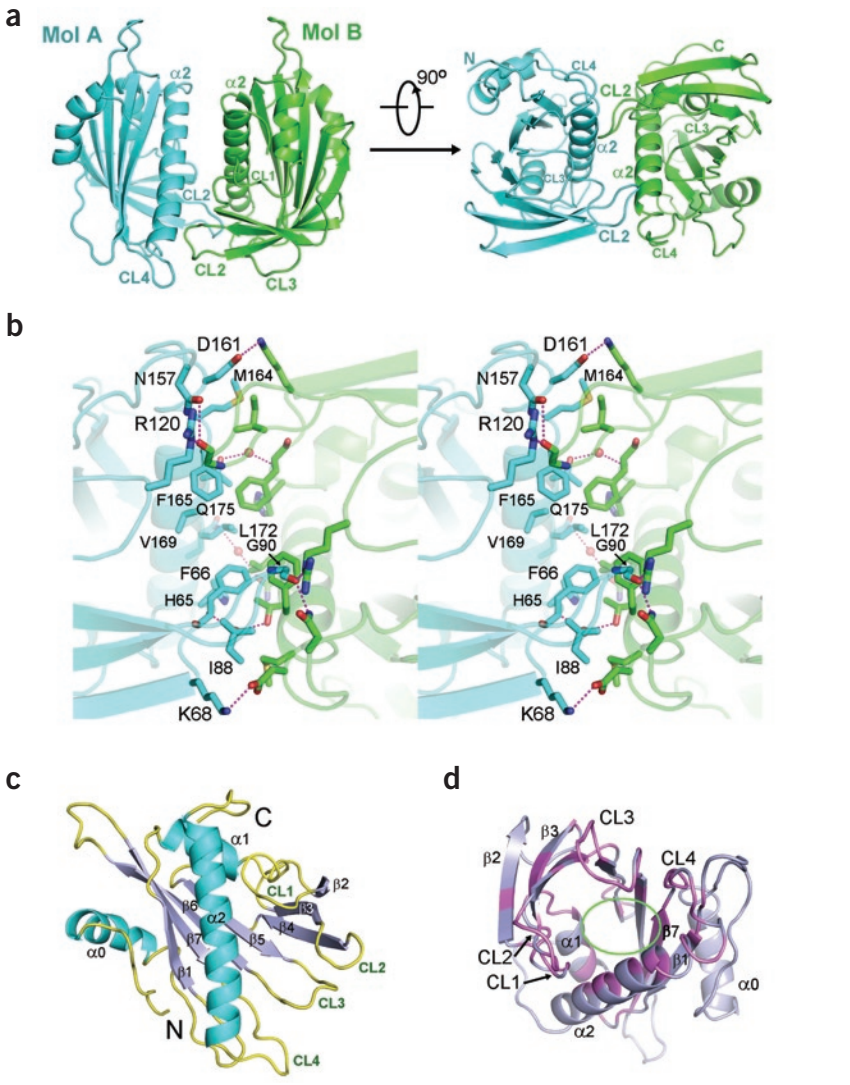

Figure 1 Structure of ABA-free PYL2. (**a**) Structure of the ABA-free PYL2 dimer in two perpendicular views. The two protomers (Mol A and Mol B) are colored cyan and green. (**b**) A stereo view of the PYL2 dimer interface. Hydrogen bonds are represented by magenta dashed lines and water molecules by red spheres. (**c**) Structure of a PYL2 protomer. PYL2 has a helix-grip fold comprising seven central β-strands and two α-helices. There is an additional α-helix (α0) at the N terminus. The secondary structural elements are color-coded. (**d**) A putative ligand-binding pocket in PYL2 is highly conserved. The conserved residues in the 14 PYL proteins are highlighted in magenta. All structure figures were prepared with PyMol (http://www.pymol.org).

(+)-ABA recognition by PYL2

In the presence of (+)-ABA, PYL2 was crystallized in the space group $P6_122$. The structure of (+)-ABA bound PYL2 was determined by molecular replacement, and the final atomic model was refined to 2.4-Å resolution (**Table 1**). The (+)-ABA molecule was built into the model after all protein atoms were in place, at which point the electron density for the (+)-ABA molecule became clearly defined (**Supplementary Fig. 3**).

There is one molecule of PYL2 in each asymmetric unit. However, two molecules from adjacent asymmetric units form a homodimer (**Fig. 2a**). The existence of such a dimer in solution is supported by the size-exclusion chromatography profile of PYL2 in the presence of (+)-ABA (**Supplementary Fig. 2e**). This is consistent with recent observations on PYR1 (ref. 16). There is one ABA molecule encaged in the conserved pocket of PYL2, with its charged carboxylate pointing into the pocket, away from the conserved loops (**Fig. 2b**). The coordination of ABA is mediated by a combination of polar and van der Waals interactions (**Fig. 2c**,**d**). At one end of the extended ABA molecule, the carboxylate accepts two hydrogen bonds from the side chain amine group of Lys64 in CL1. In addition, the carboxylate is coordinated by PYL2 indirectly through three water molecules. One water molecule mediates a maximum of four hydrogen bonds—donating two to the carboxylate of ABA and Glu147 in strand β7 and accepting two from the side chains of Tyr124 in CL3 and Ser126 in strand β6. Another water molecule donates two hydrogen bonds to the carboxylate of ABA and Glu147 and accepts one from Asn173 in helix α2. A third water molecule makes three hydrogen bonds, one to the carboxylate of ABA, one to Glu98 in strand β4, and one to the hydroxyl group of (+)-ABA. The carbonyl oxygen of (+)-ABA is coordinated by the main chain groups of Pro92 in CL2 and Arg120 in CL3 indirectly through a water molecule (**Fig. 2c**). In contrast to the charged carboxylate, the aliphatic portion of ABA is surrounded by the side chains of a number of hydrophobic amino acids, which include Phe66 in CL1; Val 87, Leu91 and Ala93 in CL2; Val114, His119, Leu121 and Tyr 124 in CL3; and Phe165, Val166, Val169 and Val170 in α2 (**Fig. 2d**). Notably, the residues that directly coordinate ABA are highly conserved among all 14 PYLs, suggesting a common mode of ABA recognition by all PYLs (**Supplementary Fig. 1**).

Table 1 Data collection and refinement statistics

	I-SAD PYL2	Native PYL2	ABA-bound PYL2	PYL1–ABI–ABA
Data collection				
Space group	$C222_1$	$C222_1$	$P6_122$	$P2_12_12_1$
Cell dimensions				
a, *b*, *c* (Å)	62.9, 107.37, 187.06	62.49,105.48, 187.91	60.92, 60.92, 253.38	61.61, 86.79, 110.7
α, β, γ (°)	90, 90, 90	90, 90, 90	90, 90, 120	90, 90, 90
Wavelength (Å)	1.54178	1.00000	1.00000	1.00000
Resolution (Å)	50–2.86 (3.03–2.86)	50–1.65 (1.71–1.65)	50–2.38 (2.47–2.38)	50–1.88 (1.95–1.88)
R_{merge} (%)	2.8 (4.9)	4.1 (21.1)	6.2 (84.2)	5.3 (59.4)
$I/\sigma I$	27.5 (14.2)	32.8 (6.5)	27.0 (2.3)	24.7 (1.9)
Completeness (%)	95.4 (81.8)	98.6 (94.4)	95.5 (97.6)	90.4 (53.2)
Redundancy	2.44	4.0	6.6	4.2
Refinement				
Resolution (Å)		50–1.65	50–2.38	50–1.88
No. reflections		73,904	11,599	40,822
R_{work} / R_{free}		17.5 / 20.0	22.6 / 27.9	21.0 / 24.8
No. atoms		5,622	1,466	3,737
Protein		4,597	1,433	3,547
Ligand/ion			19	20
Water		1,025	14	170
B-factors		26.35	72.86	60.42
Protein		23.92	73.26	60.62
Ligand/ion			63.60	54.57
Water		37.25	61.88	56.19
r.m.s. deviations				
Bond lengths (Å)		0.005	0.008	0.006
Bond angles (°)		0.941	1.142	1.015

One crystal was used for each structure. Values in parentheses are for highest-resolution shell.

The specificity of ABA recognition by PYL2 is mainly afforded by the two charge-stabilized hydrogen bonds between the carboxylate of ABA and Lys64 of PYL2 and, to a lesser extent, by the water-mediated hydrogen bonds. The binding of the aliphatic portion of ABA is mediated by the less specific hydrophobic interactions. In particular, the hydroxyl group of ABA, which determines the chiral specificity, is not specifically recognized by PYL2 but merely recognized through a water-mediated hydrogen bond (**Fig. 2c**). This is consistent with the observation that PYL2 can respond to both (+)- and (–)-ABA without chiral specificity[10]. In fact, (–)-ABA could be modeled into the PYL2 pocket without any steric clash (data not shown). Nonetheless, the recognition of the carboxylate group by Lys64 is essential, as the PYL2 mutant K64A completely abolished the binding of ABA as measured by isothermal titration calorimetry (ITC) (**Supplementary Fig. 4**).

The general mode of ABA recognition by PYL2 is reminiscent of ligand binding by other members of the PR10 family[17–19] (**Supplementary Fig. 5**), although most details, including the size and hydrophobicity of the ligand binding pocket and the ligand stoichiometry, are different. In the case of LlPR-10.2B, a classic PR-10 protein from *Lupinus luteus* (yellow lupine), three molecules of the plant hormone *trans*-zeatin are found in a large binding cleft[17] (**Supplementary Fig. 5a**, left). In contrast, only one or two zeatin molecules are found in the smaller binding pocket of the cytokinin-specific binding protein (CSBP)[20], which is not a member of the PR10 family but shares the helix-grip fold (**Supplementary Fig. 5a**). Compared to LIPR-10.2B, in PYL2 the curvature of the central β-sheet and the relative orientation of the two helices are different (**Supplementary Fig. 5b**), resulting in a much smaller binding pocket that can hold only one ABA molecule. Our structural observation is consistent with the reported ligand/protein stoichiometry determined by ITC[9,21]. This analysis shows that member proteins of the PR-10 family use a topologically conserved pocket for ligand recognition. The pocket size and the fine features of the structural elements surrounding the pocket determine the specificity of hormone perception.

CL2 as a lid for the ABA-binding pocket

The overall structures of ABA-free and ABA-bound PYL2 are quite similar, with an r.m.s. deviation of 0.7 Å over 160 Cα atoms (**Fig. 3a**). In particular, the surface loop CL2 undergoes a marked conformational rearrangement upon ABA binding, resulting in the closure of the ligand-binding pocket (**Fig. 3a**). In the ABA-free PYL2 structure, CL2 has an open, extended conformation that allows access to the ligand-binding pocket. In response to ABA binding, the Cα atoms of Leu91, Pro92 and Ala93 in the CL2 loop move toward ABA by 4.3 Å, 9.1 Å and 7.0 Å, respectively (**Supplementary Fig. 6**). Consequently, Leu91 and Ala93 are placed within van de Waals contact distances of the aliphatic portion of ABA (**Fig. 2d**), and the carbonyl oxygen of Pro92 forms a water-mediated hydrogen bond with the carbonyl group of ABA (**Fig. 2c**). In contrast to residues Leu91–Thr95, whose Cα atoms are translocated toward ABA, the Cα atom of Ser89 moves away from ABA by 4.2 Å. Moreover, the side chain of Ser89 is flipped by about 120° around the peptide bond, pointing away from the bound ABA molecule (**Fig. 3a** and **Supplementary Fig. 6**). The overall conformational shift involves a roughly 90°pivoting of the CL2 fragment Gly90–Ser94 around an axis running through residues Gly90 and Ser94 (**Supplementary Fig. 6**). These structural rearrangements result in the burial of ABA within the PYL2 molecule. Thus, CL2 serves as an open and closed lid in the ABA-free and -bound PYL2, respectively.

In the presence of ABI2, the binding affinity between PYL9 and ABA increases by about ten-fold[9]. One potential explanation is that PYL9 and ABI2 may both make direct contacts to ABA. Our current structural observations strongly argue against such a model, because ABA is completely buried within the ligand binding pocket of PYL2 and unavailable for interactions with ABI2. Our finding is consistent with a study in which no ABA bound to PP2C could be detected[22].

Functional consequences of CL2 closure

The observation that only ABA-bound, but not ABA-free, PYLs associate with PP2Cs strongly suggests that the structural differences between the apo and ABA-bound PYLs are responsible for binding to PP2Cs. Because the main structural differences observed between PYL2 with and without ABA are in the CL2 region, we hypothesized that CL2 might be essential in PP2C recognition. Closure of the ligand-binding pocket by CL2 rearranges the surface features of PYL2 and creates a relatively flat surface region (**Fig. 3a**), which we propose is responsible for PP2C association.

To corroborate this idea, we examined the impact of CL2 mutations on the ability of PYL2 to bind and to inhibit PP2Cs in the presence

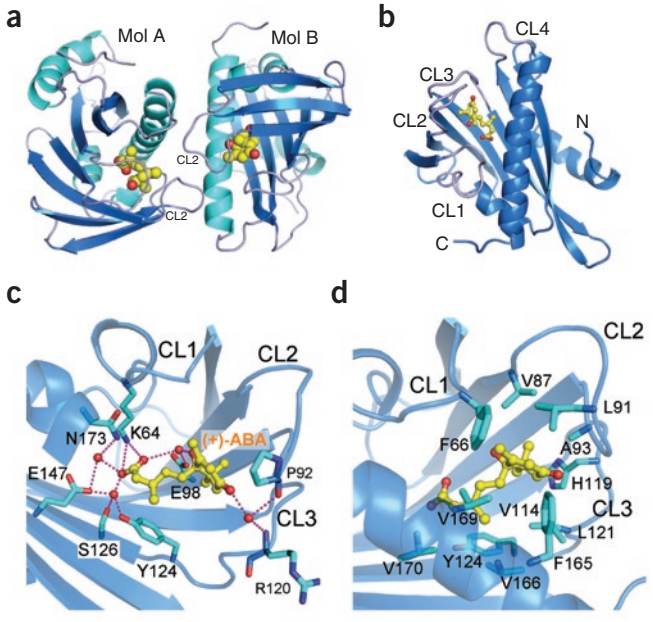

Figure 2 Structure of (+)-ABA bound PYL2. (**a**) Overall structure of the PYL2 dimer, with each promoter bound to one molecule of (+)-ABA. The protein structure is colored by secondary structural elements. ABA is shown as yellow spheres. (**b**) Structure of a PYL2 protomer in complex with (+)-ABA. (+)-ABA is shown in yellow ball-and-stick. The four conserved loops (CL1–CL4) are highlighted in light purple. (**c**) ABA recognition by PYL2 through polar interactions. The hydrogen bonds are represented by magenta dashed lines and water molecules by red spheres. The backbone of the protein is presented as semitransparent cartoon. (**d**) ABA recognition by PYL2 through van der Waals contacts.

of ABA. We did not mutate amino acids directly involved in ABA binding, such as Val87, Leu91, Pro92 and Ala93. Instead, we targeted Ser89 and Ser94, because their side chains point outward, away from the ABA binding pocket (**Fig. 3a**). A mutant PYL2 with both serine residues mutated to arginine (referred to as PYL2-S2R) bound (+)-ABA with even higher affinity than WT PYL2 (**Supplementary Fig. 4**). In contrast, PYL2-S2R had reduced interaction with ABI1 in the presence of ABA, as seen in glutathione S-transferase (GST)-mediated pulldown assay (**Fig. 3b**). The mutant K64A cannot bind ABA (**Supplementary Fig. 4**) and, as expected, did not interact with ABI1 (**Fig. 3b**).

Next, we compared the inhibitory effect of PYL2 WT and S2R on the activity of plant phosphatase ABI1 *in vitro* (**Fig. 3c**). The phosphatase activity of ABI1 was reduced by ~10% in the presence of (+)-ABA, consistent with published observations[9]. Addition of WT PYL2 and (+)-ABA completely abolished the phosphatase activity of PYL2, as reported previously[9,10] (**Fig. 3c** and **Supplementary Fig. 7**). The PYL2 mutant K64A, which (as discussed above) lacks the ability to bind ABA or ABI1, did not inhibit the phosphatase activity of ABI1 in the presence of (+)-ABA (**Fig. 3c**). In contrast, PYL2-S2R, though still able to bind ABA (**Supplementary Fig. 4c**), did not inhibit the phosphatase activity of ABI1 to the same extent as WT PYL2 (**Fig. 3c**). Together, the biochemical evidence supports a role of CL2 in the interaction of PYLs with PP2Cs.

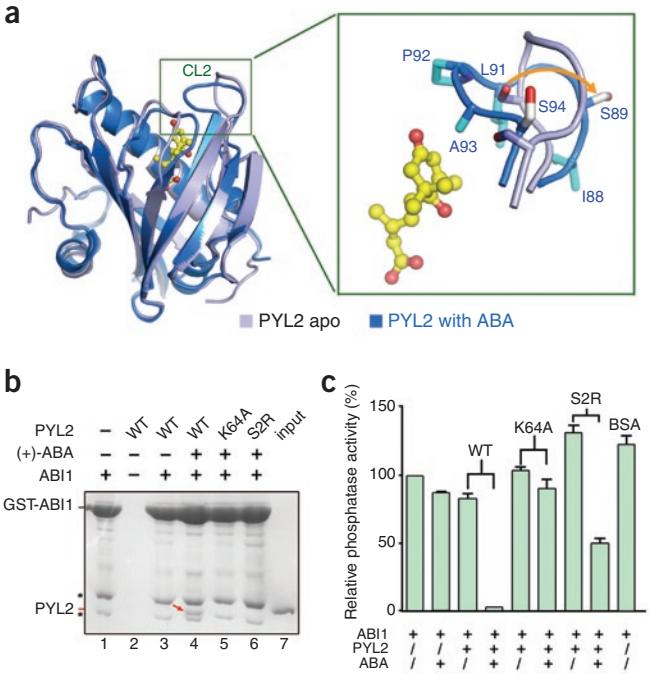

Figure 3 Structural comparison between (+)-ABA–free and (+)-ABA –bound PYL2. (**a**) Superimposition of (+)-ABA–free and –bound PYL2. A close-up view of the conformational rearrangement of CL2 is shown on the right. (**b**) The PYL2 mutations K64A and S89R/S94R (S2R) both led to loss of interaction with ABI1 in the presence of ABA, as shown by GST pulldown. PYL2 is highlighted by a red arrow. Asterisks indicate contaminating proteins on the GS4B resin. (**c**) The S2R mutation reduced the ability of PYL2 to inhibit ABI1 in the presence of ABA. The relative phosphatase activity of each reaction was normalized to that of the reaction containing substrate and ABI1 (100%). Each reaction was repeated at least six times; error bars represent s.e.m.

An altered PYL2 dimer interface upon ABA binding

The relative orientation of the two PYL2 protomers is changed upon ABA binding (**Fig. 4**). Although one molecule from each dimer can be superimposed, with an r.m.s. deviation of 0.7 Å, over 160 Cα atoms, the other molecule pivots around CL3 by ~10° (**Fig. 4a**, right). Consequently, the curvature formed by the two apo-PYL2 monomers is flattened upon ABA binding (**Fig. 4a**, left).

The change of the relative orientation between the two PYL2 protomers and the conformational change of the CL2 loop result in significant rearrangement of the interface residues. The numbers of van der Waals contacts and hydrogen bonds at the dimeric interface both decrease in response to ABA binding, resulting in a reduced buried surface area from 1,766 Å^2 to 1,478 Å^2 (**Figs. 1b** and **4b**). Hence, ABA binding appears to weaken the homodimeric interface, a change that may be functionally important. It is of particular note that CL2, the lid for the ABA binding pocket, is heavily involved—though with distinct sets of residues—in the dimer interfaces for both apo and ABA-bound PYL2 (**Figs. 1b** and **4b**).

Structure of the ABA–PYL1–ABI1 ternary complex

To further elucidate the mechanism of ABA signaling, we assembled and crystallized the ABA–PYL1–ABI1 ternary complex in the $P2_12_12_1$ space group. The structure was determined by molecular replacement and refined to 1.9-Å resolution (**Fig. 5a** and **Table 1**). (+)-ABA–bound PYL1 forms a 1:1 complex with the catalytic core domain of ABI1 (residues 118–425). One (+)-ABA molecule is enclosed in the conserved ligand-binding pocket of PYL1 (**Fig. 5**).

The catalytic core domain of ABI1 shares considerable structural homology with its mammalian and bacterial PP2C orthologs[23–26]. ABI1 contains a central β-sandwich flanked by a pair of α-helices on each side. Only one metal ion (likely to be Mn^{2+}, based on what has been reported

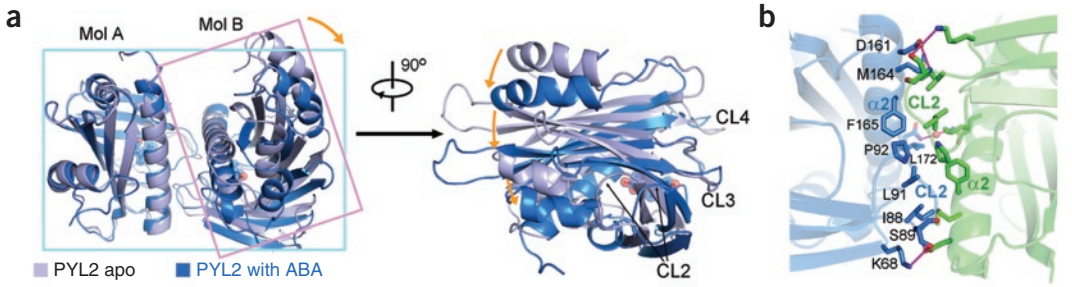

Figure 4 Structural comparison of (+)-ABA–free and (+)-ABA –bound PYL2 homodimers. (**a**) ABA binding induces a slight tilt of one PYL2 protomer relative to the other protomer. Two perpendicular views are shown. (**b**) The interface of the homodimeric, (+)-ABA–bound PYL2. Hydrogen bonds are represented as magenta lines.

in other PP2Cs) was observed in the active site of ABI1, instead of the two or three catalytic metal ions seen in other PP2C structures[23]. The ABA-bound PYL1 is located at the entrance to the active site of ABI1 (**Fig. 5b**), apparently blocking substrate entry. PYL1 shares a sequence identity of 54% with PYL2 over 172 amino acids (**Supplementary Fig. 1**). Consequently, the helix-grip fold[12] of PYL1 is identical to that of PYL2 (**Supplementary Fig. 8**).

The current structure of ABA–PYL1–ABI1, at 1.9-Å resolution, allowed accurate modeling of (+)-ABA (**Supplementary Fig. 8**). Detailed analysis revealed that the recognition of (+)-ABA by PYL1 in the ABA–PYL1–ABI1 complex is literally identical to the binding of (+)-ABA by PYL2, including the number and positions of water molecules involved (**Fig. 2** and **Supplementary Fig. 8**). (+)-ABA is buried within the conserved pocket of PYL1. There is no direct contact between ABA and ABI1, except for one water-mediated hydrogen bond between the carbonyl oxygen of ABA and the side chain of Trp300 in ABI1 (**Figs. 5b** and **6a** and **Supplementary Fig. 8c**). Similar observations have recently been reported elsewhere[27].

Interface between PYL1 and ABI1

The interaction of PYL1 with ABI1 is primarily mediated by the CL loops, especially CL2 as proposed earlier, and helix α2 of the ABA-bound PYL1 (**Fig. 6a** and **Supplementary Fig. 1**). The interaction involves a network of extensive van der Waals contacts, water-mediated hydrogen bonds and a few direct hydrogen bonds (**Fig. 6a**). Ser112 from CL2, corresponding to Ser89 in PYL2 (**Fig. 3**), appears to have a key role in mediating the interaction between PYL1 and ABI1, with its hydroxyl group donating one hydrogen bond to Glu142 of ABI1 and accepting one from the backbone amide of Gly180. The backbone amide of Gly180, in turn, makes a hydrogen bond to the backbone carbonyl oxygen of Ser112. Furthermore, a water molecule forms three hydrogen bonds with the amide and hydroxyl groups of Ser112 as well as the carboxylate of Glu142 of ABI1. Other intermolecular hydrogen bonds are formed between Pro115 and Asn301, Gly113 and Arg304, and His87 and Thr239, respectively, of PYL1 and ABI1 (**Fig. 6a**, left). The van der Waals contacts are mediated by eight amino acids from PYL1: Phe88 from CL1, Leu114 and Pro115 from CL2, Leu144 from CL3, Pro178 from CL4, and Leu188, Phe189 and Leu196 from α2; and by four residues from ABI1: Trp300, Phe306, Val308 and Tyr319 (**Fig. 6a**). Trp300 seems to be the key interfacing residue from ABI1, in that it fits perfectly into the surface cave of PYL1 (**Fig. 5b**) and contributes to both hydrophobic contacts and water-mediated hydrogen bonds with PYL1 as well as with ABA (**Fig. 6a** and **Supplementary Fig. 8c**).

The structure explains why G180D mutations in ABI1 or G168D mutations in ABI2 resulted in the loss of interaction with PYLs[9]. Gly180 of ABI1 is in close proximity to Ser112 in CL2 of PYL1, with the main chain amide group of Gly180 hydrogen bonded to Ser112 of PYL1 (**Fig. 6a**). Mutation of this glycine residue to aspartate is likely to change the conformation around this residue, causing disruption of hydrogen bonds and perhaps introducing steric hindrance into the interface between ABIs and PYLs. To support this hypothesis, we generated a mutant ABI1 protein containing the mutation

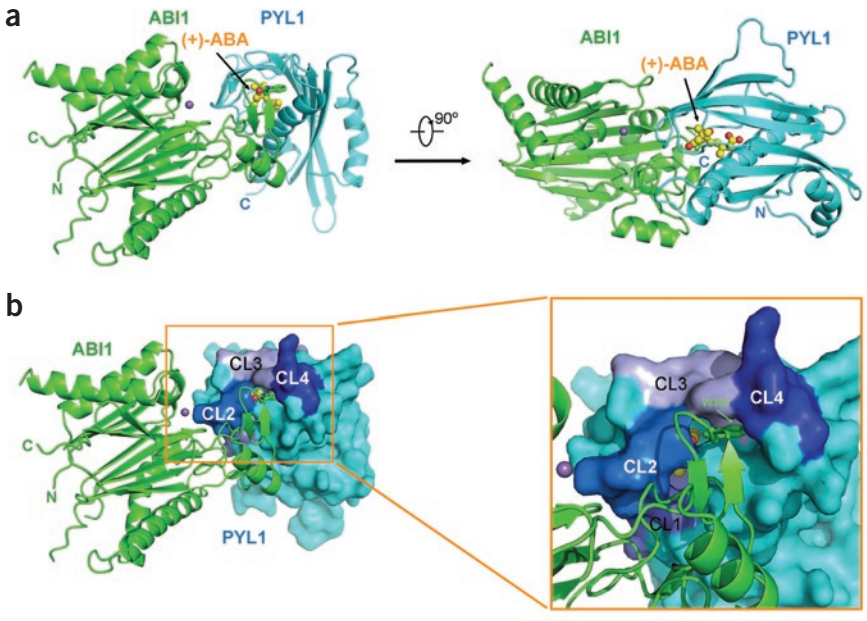

Figure 5 Structure of the (+)-ABA–bound PYL1 in complex with ABI1. (**a**) Overall structure of the (+)-ABA–bound PYL1 in complex with ABI1. Two perpendicular views are shown. There is only one metal ion (purple sphere) in the active site of each ABI1 molecule. (**b**) ABI1 does not make direct contacts to (+)-ABA. PYL1 is shown in surface representation to highlight the buried nature of (+)-ABA. The CL2 loop is in close proximity to the active site of ABI1, likely blocking entry of substrate phosphoprotein to the active site. Trp300 of ABI1 is highlighted in sticks.

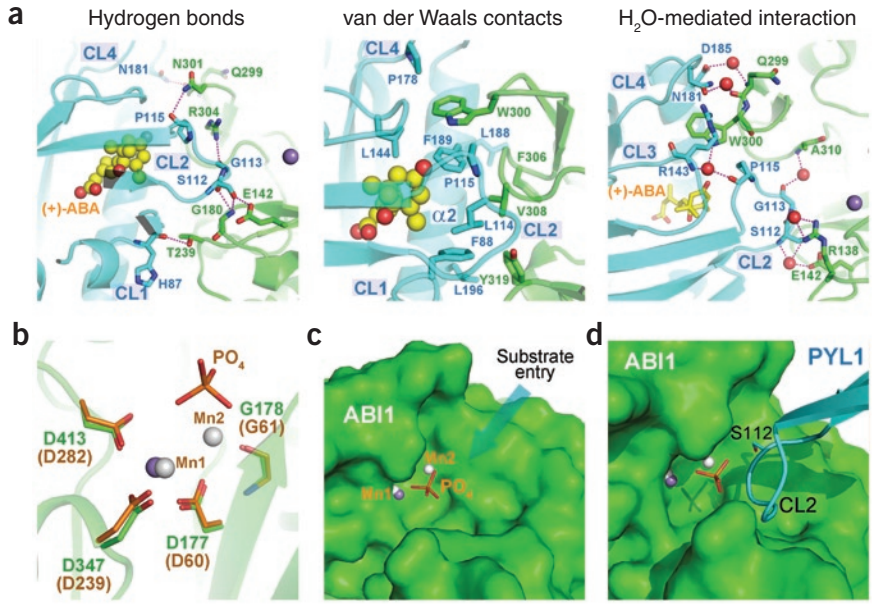

Figure 6 Recognition and inhibition of ABI1 by the (+)-ABA–bound PYL1. (**a**) The interface between ABI1 and the (+)-ABA–bound PYL1 is shown for hydrogen bonds (left), van der Waals contacts (middle) and water-mediated interactions (right). Hydrogen bonds are represented in magenta, dashed lines. The metal ion and water molecules are shown as purple and red spheres, respectively. (**b**) Superposition of the structure of ABI1 with that of the human PP2C bound to phosphate (PDB 1A6Q[24]). Shown here is a close-up view of the active site. Amino acids from ABI1 and human PP2C are colored green and orange, respectively. Metal ions from ABI1 and human PP2C are colored purple and silver, respectively. ABI1 contains only a single metal ion, whereas human PP2C contains two. (**c**) A surface view of the active site of ABI1, showing the substrate-binding groove. The two metal ions and phosphate group from human PP2C are shown in the corresponding positions in ABI1. (**d**) The CL2 loop from ABA-bound PYL1 is in close proximity to the active site of ABI1. This arrangement may block entry of substrate proteins into the active site of ABI1.

G180E. Although the phosphatase activity of WT ABI1 was completely inhibited by PYL1 or PYL2 in an ABA-dependent manner (**Fig. 3c** and **Supplementary Fig. 9a**), ABI1-G180E was no longer subject to inhibition by (+)-ABA–bound PYL1 or PYL2 (**Supplementary Fig. 9b**).

Inhibition mechanism of ABI1 by ABA–PYL1

In the ABA–PYL1–ABI1 ternary complex, the metal ion is coordinated by three aspartate residues, Asp177, Asp347 and Asp413, and corresponds to the one with a higher occupancy in the human PP2C protein[24]. The position of the metal ion and the conformations of the conserved catalytic residues are nearly identical to those of the human PP2C[24] (**Fig. 6b**). However, the CL2 loop of PYL1 is located in the close proximity of the active site of ABI1 (**Figs. 5** and **6**). This observation provides a strong indication that PYLs may exclude substrate entry into the active sites of ABIs, thereby inhibiting their phosphatase activity. We superimposed the structure of ABI1 from the ABA–PYL1–ABI1 ternary complex with that of PP2C (**Fig. 6b**) and examined the open space above the catalytic metal ion in the active site (**Fig. 6c**,**d**). This comparison revealed that the CL2 loop is positioned directly above the position occupied by the putative substrate phosphate group in the PP2C structure[24] (**Fig. 6d**). The analysis suggests that the arrangement of CL2 does not allow the access of substrate phosphoprotein to the active site of ABI1.

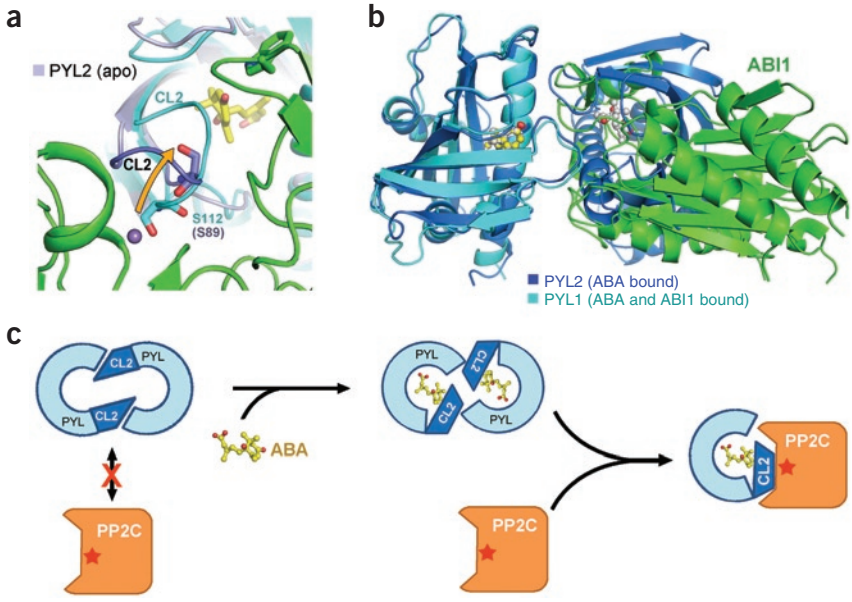

Figure 7 A working model for ABA-dependent recognition and inhibition of PP2Cs by PYLs. (**a**) The conformation of the CL2 loop in the ABA-free PYL2 (light purple) is incompatible for binding to ABI1 (green). Ser112 in PYL1 (cyan), which corresponds to Ser89 in PYL2, plays an essential role in the interface between PYL1 and ABI1. It is in an incompatible position for binding to ABI1 in apo-PYL2. The metal ion indicating the active site of ABI1 is shown as a purple sphere. (**b**) Superimposition of the dimeric, (+)-ABA bound PYL2 with (+)-ABA–PYL1–ABI complex. There is significant structural overlap between ABI1 and a PYL2 protomer, explaining why ABI1 forms a 1:1 complex with the (+)-ABA–bound PYL1. Note that the structure of (+)-ABA bound PYL2 is almost identical to that of the PYL1 in the (+)-ABA–PYL1–ABI1 complex. (**c**) A working model for ABA-dependent recognition and inhibition of PP2Cs by PYLs.

DISCUSSION

Why is ABA required for PYLs to bind and inhibit PP2Cs? As we proposed earlier, ABA binding induces a major conformational change in the CL2 loop, which plays an essential role in the recognition and inhibition of ABI1. Indeed, structural overlay of apo-PYL2 monomer and the ABA–PYL1–ABI1 complex showed that the conformation of CL2 in apo-PYL2 was incompatible with binding to ABI1 (**Fig. 7a** and **Supplementary Fig. 10a**). Notably, the structure of ABA-bound PYL2 is almost identical to that of PYL1 in the ABA–PYL1–ABI1 complex (**Fig. 7b** and **Supplementary Fig. 10b**). This observation suggests that once ABA has bound, PYLs are in a conformation ready for PP2C recognition and inhibition. Given that CL2 is a surface loop, one may question why ABI1 does not bind CL2 in apo-PYLs via an induced fit mechanism. Our structural data provide two clues. First, CL2 is involved in the dimer interface of apo-PYL2, and therefore it is not a flexible loop with conformational plasticity (**Fig. 1a**,**b**, and

Supplementary Fig. 10c). Second, residue Ser89 in PYL2 (corresponding to Ser112 in PYL1), which plays a key part in the interaction with ABI1, is not exposed on the surface in the apo-PYL2 dimer (**Supplementary Fig. 10c**) and thus cannot be recognized by ABI1.

Notably, apo and ABA-bound PYL2 both exist as dimers (**Supplementary Fig. 2e**). However, ABA-bound PYL1 forms a 1:1 heterodimer with ABI1. Structural superposition of the ABA-bound PYL2 dimer with the ABA–PYL1–ABI1 complex reveals significant overlap between one PYL2 molecule and the ABI1 phosphatase (**Fig. 7b**). Therefore, formation of the ABA–PYL1–ABI1 complex must be preceded by dissociation of the ABA-bound PYL1 homodimer. As discussed earlier, ABA-binding may result in a weakened dimer interface of PYLs (**Figs. 1b** and **4b**), thus facilitating the replacement of one PYL protomer by ABI1. Compared to the dimer interface of ABA-bound PYL2 (**Supplementary Fig. 10d**), the interface between ABA-bound PYL1 and ABI1 has better complementarities (**Supplementary Fig. 10e**).

Our structural and biochemical observations provide insight into PYL-mediated ABA signaling and give rise to a working model (**Fig. 7c**). In the absence of ABA signaling, PP2Cs are fully active and PYLs exist as inactive homodimers in cells, unable to bind or inhibit PP2Cs, mainly due to the incompatible conformation of CL2 loop. In response to ABA binding, the CL2 loop undergoes a conformational rearrangement to close onto the ABA-bound pocket. This conformational change is likely to serve two purposes. First, it generates a novel surface epitope for interactions with ABI1 (**Fig. 3**). Second, it is thought to weaken the homodimeric interface of PYLs (**Fig. 4**), a change that facilitates subsequent dissociation of the PYL dimer and formation of a 1:1 PYL1-ABI1 complex. The ABA-bound PYLs bind PP2Cs, again via the conserved CL2 loop. Binding of ABA-bound PYLs results in the complete inhibition of the phosphatase activity of PP2Cs due to the blockade of substrate entry.

The structures of ABA-free and (+)-ABA–bound PYL2 presented in this report unambiguously confirm that PYLs are ABA receptors rather than co-receptors. ABA is buried within the conserved pocket of PYLs. The advent of structural information on apo-PYLs, ABA-bound PYLs and the ABA–PYL–ABI ternary complex reveals the mechanisms of PYL-mediated ABA signaling and serves as a framework for understanding past and future biological observations.

METHODS

Methods and any associated references are available in the online version of the paper at http://www.nature.com/nsmb/.

Accession codes. The atomic coordinates of ABA-free PYL2, ABA-bound PYL2 and the ABA–PYL1–ABI1 complex have been deposited in the Protein Data Bank (PDB) with the accession codes 3KDH, 3KDI and 3KDJ, respectively.

Note: Supplementary information is available on the Nature Structural & Molecular Biology website.

ACKNOWLEDGMENTS

We thank D. Zhang for providing the *A. thaliana* cDNA library; N. Shimizu, S. Baba and T. Kumasaka at the Spring-8 beamline BL41XU for on-site assistance; J. He and S. Huang for crystal screening at Shanghai Synchrotron Radiation Facility (SSRF); and Y. Shi for critical reading of the manuscript. This work was supported by funds from the China Ministry of Science and Technology (grant 2009CB918802), Tsinghua University 985 Phase II funds, Yuyuan Foundation and Li's Foundation.

AUTHOR CONTRIBUTIONS

P.Y., H.F., Q.H., X.Y., D.W., Y.P. and W.L. performed experiments and analyzed data. C.Y., J.W. and N.Y. analyzed data. N.Y. wrote the manuscript.

Published online at http://www.nature.com/nsmb/.
Reprints and permissions information is available online at http://npg.nature.com/reprintsandpermissions/.

1. Fedoroff, N.V. Cross-talk in abscisic acid signaling. *Sci. STKE* **2002**, RE10 (2002).
2. Finkelstein, R., Reeves, W., Ariizumi, T. & Steber, C. Molecular aspects of seed dormancy. *Annu. Rev. Plant Biol.* **59**, 387–415 (2008).
3. Schroeder, J.I. & Nambara, E. A quick release mechanism for abscisic acid. *Cell* **126**, 1023–1025 (2006).
4. Shen, Y.Y. *et al.* The Mg-chelatase H subunit is an abscisic acid receptor. *Nature* **443**, 823–826 (2006).
5. Liu, X. *et al.* A G protein–coupled receptor is a plasma membrane receptor for the plant hormone abscisic acid. *Science* **315**, 1712–1716 (2007).
6. Pandey, S., Nelson, D.C. & Assmann, S.M. Two novel GPCR-type G proteins are abscisic acid receptors in *Arabidopsis*. *Cell* **136**, 136–148 (2009).
7. McCourt, P. & Creelman, R. The ABA receptors—we report you decide. *Curr. Opin. Plant Biol.* **11**, 474–478 (2008).
8. Pennisi, E. Plant biology. Stressed out over a stress hormone. *Science* **324**, 1012–1013 (2009).
9. Ma, Y. *et al.* Regulators of PP2C phosphatase activity function as abscisic acid sensors. *Science* **324**, 1064–1068 (2009).
10. Park, S.Y. *et al.* Abscisic acid inhibits type 2C protein phosphatases via the PYR/PYL family of START proteins. *Science* **324**, 1068–1071 (2009).
11. van Loon, L.C., Rep, M. & Pieterse, C.M. Significance of inducible defense-related proteins in infected plants. *Annu. Rev. Phytopathol.* **44**, 135–162 (2006).
12. Iyer, L.M., Koonin, E.V. & Aravind, L. Adaptations of the helix-grip fold for ligand binding and catalysis in the START domain superfamily. *Proteins* **43**, 134–144 (2001).
13. Allen, G.J., Kuchitsu, K., Chu, S.P., Murata, Y. & Schroeder, J.I. *Arabidopsis* abi1–1 and abi2–1 phosphatase mutations reduce abscisic acid-induced cytoplasmic calcium rises in guard cells. *Plant Cell* **11**, 1785–1798 (1999).
14. Yoshida, T. *et al.* ABA-hypersensitive germination3 encodes a protein phosphatase 2C (AtPP2CA) that strongly regulates abscisic acid signaling during germination among *Arabidopsis* protein phosphatase 2Cs. *Plant Physiol.* **140**, 115–126 (2006).
15. Rodriguez, P.L. Protein phosphatase 2C (PP2C) function in higher plants. *Plant Mol. Biol.* **38**, 919–927 (1998).
16. Nishimura, N. *et al.* Structural mechanism of abscisic acid binding and signaling by dimeric PYR1. *Science* published online, doi:10.1126/science.1181829 (22 October 2009).
17. Fernandes, H. *et al.* Lupinus luteus pathogenesis-related protein as a reservoir for cytokinin. *J. Mol. Biol.* **378**, 1040–1051 (2008).
18. Fernandes, H. *et al.* Cytokinin-induced structural adaptability of a *Lupinus luteus* PR-10 protein. *FEBS J.* **276**, 1596–1609 (2009).
19. Marković-Housley, Z. *et al.* Crystal structure of a hypoallergenic isoform of the major birch pollen allergen Bet v 1 and its likely biological function as a plant steroid carrier. *J. Mol. Biol.* **325**, 123–133 (2003).
20. Pasternak, O. *et al.* Crystal structure of *Vigna radiata* cytokinin-specific binding protein in complex with zeatin. *Plant Cell* **18**, 2622–2634 (2006).
21. Santiago, J. *et al.* Modulation of drought resistance by the abscisic acid receptor PYL5 through inhibition of clade A PP2Cs. *Plant J.* published online, doi:10.1111/j.1365-313X.2009.03981.x (16 July 2009).
22. Leube, M.P., Grill, E. & Amrhein, N. ABI1 of *Arabidopsis* is a protein serine/threonine phosphatase highly regulated by the proton and magnesium ion concentration. *FEBS Lett.* **424**, 100–104 (1998).
23. Shi, Y. Serine/threonine phosphatases: mechanism through structure. *Cell* **139**, 468–484 (2009).
24. Das, A.K., Helps, N.R., Cohen, P.T. & Barford, D. Crystal structure of the protein serine/threonine phosphatase 2C at 2.0 Å resolution. *EMBO J.* **15**, 6798–6809 (1996).
25. Schlicker, C. *et al.* Structural analysis of the PP2C phosphatase tPphA from *Thermosynechococcus elongatus*: a flexible flap subdomain controls access to the catalytic site. *J. Mol. Biol.* **376**, 570–581 (2008).
26. Barford, D., Das, A.K. & Egloff, M.P. The structure and mechanism of protein phosphatases: insights into catalysis and regulation. *Annu. Rev. Biophys. Biomol. Struct.* **27**, 133–164 (1998).
27. Miyazono, K. *et al.* Structural basis of abscisic acid signalling. *Nature* advance online publication, doi:10.1038/nature08583 (23 October 2009).

ONLINE METHODS

Protein preparation and crystallization. PYL2 (AT2G26040), ABI1 (AT4G26080), ABI2 (AT5G57050), and other PYLs and PP2Cs[10] were subcloned from the *Arabidopsis thaliana* cDNA library using standard PCR-based protocol. All mutants of PYL1 and PYL2 were generated with two-step PCR and verified by sequencing. The WT and all the mutants of PYL1 and PYL2 were expressed in *Escherichia coli* strain BL21(DE3) using the vector pET-15b induced at 18 °C for 16 h. The individual proteins were purified with Ni-NTA resin (Qiagen) followed by anion exchange chromatography (Source-15Q, GE Healthcare) and size-exclusion chromatography (Superdex-200, GE Healthcare). PP2C homologs were engineered into pGEX2T vector, overexpressed in *E. coli* BL21 (DE3) and purified with GS4B resin (GE Healthcare).

To obtain a stable ABI1–PYL1 complex, the His_6-tagged core domain (residues 118–425) of ABI1 was coexpressed with PYL1 (residues 19–210) in *E. coli* BL21(DE3). Just before IPTG induction, 4 mM $MnCl_2$ were added to the culture medium. After induction at 22 °C for 14 h, cells were collected and lysed in a buffer containing 150 mM NaCl, 25 mM Tris, pH 8.0. and 0.2 mM (+)-ABA (Jingkehongda Ltd.). The soluble fraction was purified using Ni-NTA resin (Qiagen) followed by an anion-exchange column (Source-15Q, GE Healthcare) and size-exclusion column (Superdex-200, GE Healthcare).

Crystals were grown at 18 °C using the hanging-drop vapor diffusion method. Apo-PYL2 was concentrated to 10 mg ml^{-1} and crystallized in the well buffer containing 1 M sodium citrate tribasic, 100 mM Tris, pH 8.5, and 79 mM octanoyl-*N*-methylglucamide (MEGA-8). To obtain crystals of ABA-bound PYL2, 0.6 mM (+)-ABA (Sigma-Aldrich) was mixed with 0.2 mM PYL2 for cocrystallization. Diamond-shaped crystals appeared overnight in the well buffer containing 4 M sodium formate and grew to full size in 2 d. For crystallization of the PYL1–ABI1 complex, 0.2 mM (+)-ABA (Sigma-Aldrich) was mixed with 0.1 mM protein complex. Crystals were grown in the well buffer contained 0.1 M citric acid, pH 5.5, 0.01 M glutathione (GSH/GSSG) and 10% PEG-4000. Crystals grew to full size after a week.

Data collection, structure determination and refinement. Iodine-soaked PYL2 SAD data were collected on the Rigaku Saturn 944+ CCD configured with the Rigaku MicroMax-007HF generator, integrated and scaled using the XDS package[28]. All native data were collected at the Spring-8 beamline BL41XU and processed with the HKL2000 package[29]. Further processing was carried out using programs from the CCP4 suite[30]. Data collection statistics are summarized in **Table 1**.

The iodine positions in the I-SAD PYL2 data were determined using the program SHELXD[31]. The identified heavy atoms were refined and initial phases were generated in the program PHASER[32] with the SAD experimental phasing module. The real-space constraints were applied to the SAD electron density with DM[33]. A crude model was traced automatically using the program BUCCANEER[34]. Manual model building and refinement were performed iteratively with COOT[35] and PHENIX[36].

The monomer model obtained above was used for molecular replacement with the program PHASER into the data for apo-PYL2 and ABA-bound PYL2. Both structures were refined with PHENIX. For the apo-PYL2, 90.1%, 8.7%, 1.0% and 0.2% of the amino acids in the final atomic model reside in the most favorable, additional allowed, generously allowed and disallowed regions of the Ramachandran plots, respectively. For the ABA-bound PYL2, 85.0%, 14.4%, 0.6% and 0.0% of the amino acids in the final atomic model reside in the most favorable, additional allowed, generously allowed and disallowed regions of the Ramachandran plots, respectively.

Atomic coordinates of the ABA-bound PYL2 and human PP2C (PDB 1A6Q) were used for molecular replacement, with the program PHASER[32], into the ABA–PYL1–ABI1 complex data. Manual model adjustment and structural refinement were performed with COOT[35]and PHENIX[36], respectively. 90.4%, 9.1%, 0.5% and 0.0% of the amino acids in the final atomic model reside in the most favorable, additional allowed, generously allowed and disallowed regions of the Ramachandran plots, respectively.

Size exclusion chromatography. The WT or mutant PYL2 were applied to Superdex-200 HR10/30 (GE Healthcare) in a buffer containing 25 mM HEPES, pH 7.5, and 150 mM NaCl. To examine the oligomerization state of ABA-bound PYL2, 0.2 mM WT PYL2 was incubated with 0.4 mM (+)-ABA at 4 °C for half an hour and then applied to Superdex-200 resin in the buffer either with or without 0.4 mM (+)-ABA. The proteins were visualized by SDS-PAGE followed by Coomassie blue staining.

Isothermal titration calorimetry (ITC) assays. 1 mM (+)-ABA dissolved in the reaction buffer containing 20 mM HEPES, pH 7.5, and 150 mM NaCl was titrated against 30 μM WT or mutant PYL2 proteins in the same buffer. The experiments were performed with VP-ITC Microcalorimeter (MicroCal). Thermodynamic constants were determined with Origin (version 7.0) software. The stoichiometry between ligand and protein was set to 1.0 for all the analyses.

GST-mediated pulldown assay. 200 μg of GST-fusion ABI1 protein was immobilized on glutathione S-Sepharose 4B (GS4B, GE Healthcare) resin. 50 μg of WT or mutant PYL2 proteins, pretreated with (+)-ABA, were incubated with the ABI1-bound resin for 30 min at room temperature. The resin was then extensively rinsed with buffer containing 20 mM HEPES, pH 7.5, and 150 mM NaCl to remove unbound proteins. The resin was resuspended with 200 μl of the same wash buffer. 10 μl of the suspension was taken out and applied to SDS-PAGE for analysis. The proteins were visualized with Coomassie blue staining.

Phosphatase activity assay. The phosphatase activity was measured by the serine-threonine phosphatase assay system (Promega). Each reaction was performed in a 50-μl reaction volume containing 7 μg ABI1, 20 mM HEPES, pH 7.5, and 150 mM NaCl. 10.5 μg WT or mutant PYL1 or PYL2 proteins and 10 μM (+)-ABA (Sigma-Aldrich) were added if required. After incubation with peptide substrate (supplied with the Promega kit) at 30 °C for 30 min, the reaction was stopped by addition of 50 μl molybdate dye. Absorbance at 630 nm was measured 15 min after the addition of molybdate dye.

28. Kabsch, W. Evaluation of single-crystal X-ray diffraction data from a position-sensitive detector. *J. Appl. Crystallogr.* **21**, 916–924 (1988).
29. Otwinowski, Z. & Minor, W. Processing of X-ray diffraction data collected in oscillation mode. *Methods Enzymol.* **276**, 307–326 (1997).
30. Collaborative Computational Project. The CCP4 suite: programs for protein crystallography. *Acta Crystallogr.* **D50**, 760–763 (1994).
31. Schneider, T.R. & Sheldrick, G.M. Substructure solution with SHELXD. *Acta Crystallogr. D Biol. Crystallogr.* **58**, 1772–1779 (2002).
32. McCoy, A.J. *et al.* Phaser crystallographic software. *J. Appl. Crystallogr.* **40**, 658–674 (2007).
34. Cowtan, K. DM: An automated procedure for phase improvement by density modification. *Joint CCP4 ESF-EACBM Newslett. Protein Crystallography* **31**, 34–38 (1994).
34. Cowtan, K. The Buccaneer software for automated model building. *Acta Crystallogr. D* **62**, 1002–1011 (2006).
35. Emsley, P. & Cowtan, K. Coot: model-building tools for molecular graphics. *Acta Crystallogr. D Biol. Crystallogr.* **60**, 2126–2132 (2004).
36. Adams, P.D. *et al.* PHENIX: building new software for automated crystallographic structure determination. *Acta Crystallogr. D Biol. Crystallogr.* **58**, 1948–1954 (2002).

doi: 10.1038/nsmb.1730